PHYSICAL REVIEW E **73**, 040601(R) (2006)

Defect-mediated stripe reordering in wrinkles upon gradual changes in compression direction

Takuya Ohzono[1] and Masatsugu Shimomura[1,2]
[1]*Dissipative-Hierarchy Structures Laboratory, Frontier Research System, RIKEN, 2-1 Hirosawa, Wako, Saitama 351-0198, Japan*
[2]*Research Institute for Electronic Science, Hokkaido University, N21W10, Sapporo 001-0021, Japan*
(Received 30 January 2006; published 26 April 2006)

We study the stripe rearrangements in microwrinkles subjected to gradual changes in the compression direction. The spatially averaged stripe orientation follows the changing compression direction with a deviation of 3°–4°. Meanwhile, the local stripe orientation stays constant for a certain period and a dislocation gliding nearby causes it to jump suddenly in the direction of compression. This sequence repeatedly occurs over the surface. The regular pattern transiently appears in the stripe orientation as a result of the organized glide motions, indicating the interaction between dislocations.

DOI: 10.1103/PhysRevE.73.040601 PACS number(s): 68.43.−h, 89.75.Kd, 61.41.+e, 64.60.My

Stripe patterns are ubiquitous in nature [1–3]. Patterns arrange themselves by self-organization. Interactions between components of the system give rise to spontaneous patterns. Wrinkles on some compliant materials (e.g., elastomers), whose surface skins (layers) are harder than the bulk, show such stripe patterns of surface undulations. The wrinkle forms as the result of Euler buckling when the surface layer is compressed [4–9]. Recently, wrinkles on nanometer-micrometer scales have been extensively studied experimentally [10–19] for their potential impacts on technological applications, e.g., templates for micropatterning, optical devices, and cell culture substrates. These studies mainly focus on the control of pattern formation and/or the intrinsic nature of relaxation to the static states.

In general, the response of a system to a perturbation indicates the state's stability and nonlinearity. Thus, our recent studies have focused on microwrinkles' responses to mechanical perturbations [20–23]. We observed reversible ordering of random [20] and aligned [21] stripe patterns by applying uniaxial compressive strains. For sufficiently small strains, wrinkles behave like elastic springs and are capable of supporting static strains. This behavior can be understood in terms of the linear response of individual parts on wrinkles. When the strain is sufficiently large, some local parts of the surface suddenly deform (rebuckling), thereby changing the stripe orientations. This nonlinear behavior involves topological rearrangements, such as the motions of defects, in the stripe pattern from one metastable state to another [24]. Thus, the domains of aligned stripes in the compression direction form and grow as the strain increases. These studies revealed the connection between topological rearrangements of stripes and the statistical properties of stripe orientations under gradual changes in the uniaxial compressive strain.

Another mechanical perturbation of great interest is to gradually change the compression direction as the degree of compressive strain remains constant. The changes can be expressed by the clockwise (CW) or counterclockwise (CCW) rotation of the director vector of the compression direction with the length kept constant. In this system, it can be predicted from the previous studies that the average stripe orientation follows the gradually changing compression direction. However, for the system of interest, the relationship between the strain field change, the stripe orientation changes, and the topological rearrangements, such as the defect motions (dislocation glide), remains unclear.

We report the first observations of stripe rearrangements in microwrinkles under gradual changes in the compression direction. The microwrinkles on a Pt-coated elastomer are used; they show stripes with an average spatial wavelength $\lambda = 1.1$ μm. The stripe rearrangements are observed at different fixed values of the compressive strain. The observed patterns are analyzed in terms of the stripe orientation at each location [25] and in terms of the defect motions. The connection between the organized defect motions (dislocation glide) and the stripe rearrangement is discussed.

The sample used is a 5-mm-thick right circular cylinder with a diameter of 10 mm. A hard skin is formed through Pt deposition on one side, which is a flat circular surface [20,23]. First, the sample is compressed in a vise to form an aligned stripe pattern. The left plate of the vise is slid in the perpendicular direction to rotate the sample with the compressive strain kept constant [Fig. 1(a)] at different values: 5, 7, and 9% [26]. The motion of the left plate in the upside (or downside) direction invokes the CW (or CCW) rotation of the sample with respect to the compression direction that corresponds to the x axis in Fig. 1(a). That is, the compression direction can be gradually changed. The rotational angle ϕ is defined in Fig. 1(a); it is the angle between the x axis and the reference direction arbitrarily fixed on the sample surface. The slow CW rotation (less than 0.1°/s) is started from the point with $\phi = 63°$ to the point with $\phi = -17°$. Then, the CCW rotation begins and ϕ finally returns to the initial value, $\phi = 63°$. The rotation is stopped to allow the system to

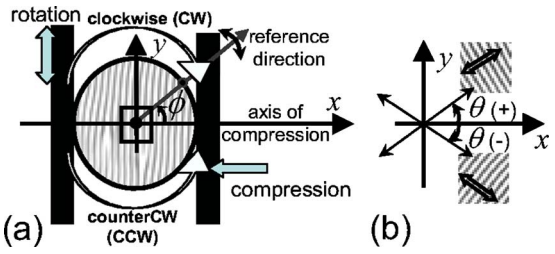

FIG. 1. (Color online) (a) Schematic of the experimental setup. The square located at the center of the sample schematically indicates the area (58×58 μm^2) observed. (b) Schematic for the definition of θ.

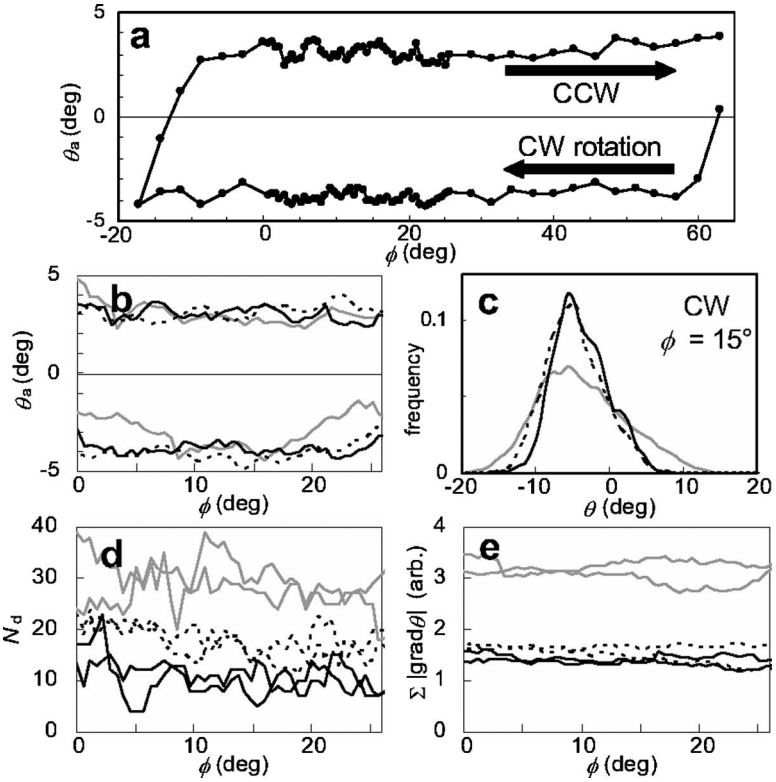

FIG. 2. Statistical quantities. (a) Evolution of θ_a at compressive strain 9% during a whole cycle of the CW and CCW rotations. (b) Evolutions of θ_a at different strains on the steady states. (c) Histograms of θ at different strains at $\phi=15°$ on the CW rotation. (d) and (e) Evolutions of N_d and the sum of $|\text{grad}(\theta)|$ at different compressive strains on the steady states, respectively. The solid, dashed, and gray lines indicate data at compressive strains of 5, 7, and 9%, respectively.

equilibrate for 30 s before each image acquisition. The data acquired on the steady states between $\phi=0$ and 25° are analyzed in detail.

The stripe orientation θ is calculated at each point in the image ($n=512^2$ pixels) based on the method by Egolf *et al.* [25], where θ is the angle between the wave director and the x axis, and is defined within a range from −90° to 90° due to the C_2 symmetricity [Fig. 1(b)]. The average value of θ over an image of interest (58×58 μm^2) is calculated by $\theta_a=\{\tan^{-1}[\langle\cos(2\theta)\rangle/\langle\sin(2\theta)\rangle]\}/2$, where the bracket, $\langle p\rangle$, is the simple average over n pixels. The value of $|\text{grad}(\theta)|$ is calculated at each point [27] to count the number of dislocations, N_d. The sum of $|\text{grad}(\theta)|$ over n pixels is also calculated and serves as a rough index of the total number of defects, including dislocations and phase grain boundaries (PGBs).

The almost-aligned stripes with $\theta_a\approx0°$ [Fig. 2(a)] appear after the first uniaxial compression. The patterns are not perfect stripes but show dislocations. In contrast to the simulations [8], it is difficult to obtain perfect stripes. The inherent imperfections, such as roughness and uneven density distribution, probably prevent the defects from disappearing by pinning them.

As the CW rotation of the sample begins, θ_a linearly decreases. The stripes barely rearrange in this initial period, indicating that the wrinkles respond linearly to the change in the compression direction. Although there might be a slight (linear) deformation in this period, it is too small to be detected. After a CW rotation of approximately −4° ($\phi=60°$), θ_a starts to show steady values, $\theta_a\approx-4°$. The stripes rearrange with λ kept constant during this steady period. Then, the CCW rotation of the sample is started at $\phi=-17°$. First, θ_a linearly increases without stripe rearrangement; this behavior is similar to that observed in the initial period of the CW rotation. The stripes start rearranging from $\phi=-10°$ on the CCW rotation, showing the steady state with $\theta_a\approx3°$. This result indicates hysteretic behavior, where different patterns appear depending on the history of the change in the compression direction (CW or CCW). This is consistent with the previous results that the microwrinkle pattern can have many metastable states [20,21,23].

The evolutions of θ_a during the steady states for cases with different compressive strains are shown in Fig. 2(b), indicating little difference between them. The absolute values of the deviation of θ_a from 0° (compression direction) are in the range of 3°–4°. However, the pattern at a low compressive strain (5%) shows a wider distribution of θ than those at high strains (7% and 9%) [Fig. 2(c)]. We find this trend in the distribution of θ at any value of ϕ.

The distribution difference is predictable from the optical and analyzed images during the CW rotation in Fig. 3. The lines of stripes at low compression are more curved than those at high compression [Figs. 3(a)–3(c)]. The wide distribution in θ generally indicates that the stripe pattern shows topological defects [2]. In the present system, we observe dislocations and blurred PGBs. The latter boundary lines appear mainly in the slightly tilted direction with respect to the x axis, showing the blurred stripes in images of θ [Figs. 3(d) and 3(e)]. The relatively dense PGBs (blurred stripes) and high contrast at low compression can be clearly seen. The number of dislocations, N_d, and the sum of $|\text{grad}(\theta)|$ are shown in Figs. 2(d) and 2(e), respectively. Both N_d and the sum of $|\text{grad}(\theta)|$ are larger at low compression than at high compression. These results correlate with the difference in the distribution in θ.

Figure 4 shows the evolutions of θ at a fixed location at

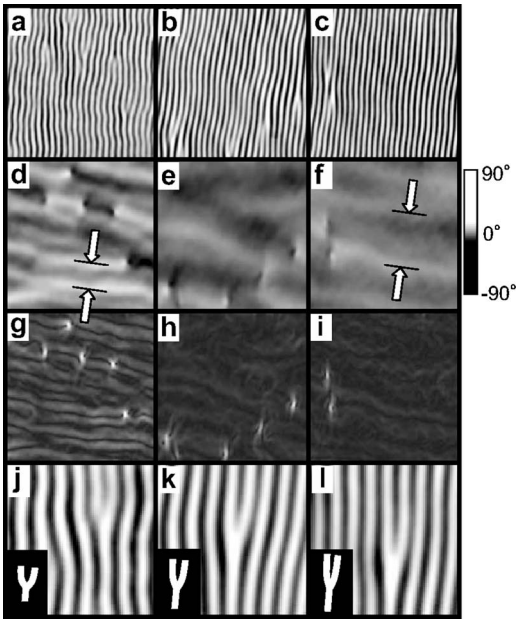

FIG. 3. Images obtained during the CW rotation. (a)–(c) Optical images (27×27 μm^2). (d)–(f) Images of θ calculated from (a)–(c), respectively. (g)–(i) Images of $|\mathrm{grad}(\theta)|$ calculated from (a)–(c), respectively. (j)–(l) Magnified optical images (9.3×9.3 μm^2) showing the dislocations with the schematics (insets). The left, middle, and right columns are images at 5, 7, and 9% strains, respectively. Arrows indicate the periodic distance of the secondary structure.

different compressive strains. The sawtooth behaviors indicate that the local stripe orientation just linearly changes, owing to the sample rotation for a certain period, and suddenly jumps toward the compression direction. Although we observe sawtooth behaviors everywhere on the area of interest, the phases deviate depending on the location. Thus, the behavior is averaged out in θ_a. Meanwhile, please note that all of the local stripe rearrangements in this system are strongly related to the sudden jumps in θ.

We found that the jump in θ occurs when a dislocation passes (glides) nearby at the location of interest. Figure 5 shows a typical dislocation life cycle. This is repeatedly found everywhere in the images during the steady state on CW rotation. A pair of dislocations carrying an opposite charge (Burger's vector) forms at the location that shows a relatively large deviation in θ from 0 (the compression direction). The dislocations travel (glide) in the opposite lateral directions, changing θ toward 0. Finally, the dislocation is annihilated by colliding with another dislocation having the opposite charge, when the distance between the lines of their glide trajectories is sufficiently small ($\approx\lambda$).

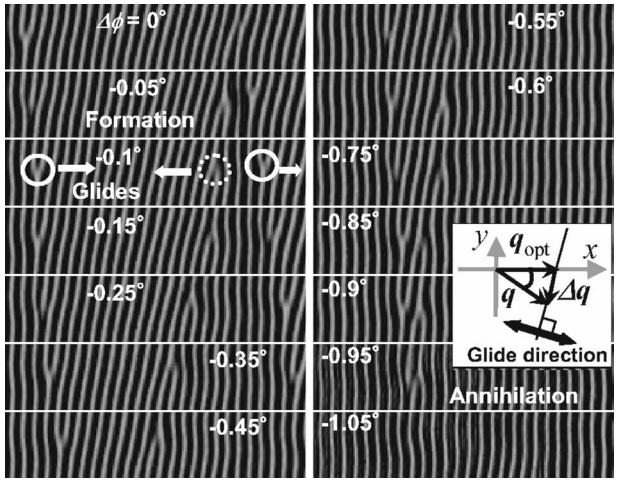

FIG. 5. Sequential images (29×6.5 μm^2) observed on the CW rotation with a 7% strain. Formation, glide motions, and annihilation of dislocations are identified. Note that the stripe orientation jumps to the optimal direction after the dislocation passes. (Inset) The relation between $\mathbf{q}$, $\mathbf{q}_{\mathrm{opt}}$, $\Delta\mathbf{q}$, and the direction of the glide motion.

Glide motions similar to those observed have been found in the stripe patterns of the fluid system with convective rolls [28,29]; the dislocation glide is interpreted as the selection process of the stripe orientation. According to those previous studies, we can predict the direction of the dislocation glide, which is perpendicular to the vector, $\Delta\mathbf{q}=\mathbf{q}-\mathbf{q}_{\mathrm{opt}}$, where $\mathbf{q}$ and $\mathbf{q}_{\mathrm{opt}}$ are the temporal and optimal wave vectors of the stripes, respectively. We found that the prediction also holds in the present system as follows. The vector $\Delta\mathbf{q}$ normalized by λ^{-1} reads $(\cos\theta-1, \sin\theta)$. Assuming the deviation in θ as $-4°$ $(+4°)$ for the CW (CCW) rotation, $\Delta\mathbf{q}\approx[-0.002, -0.070\ (+0.070)]$. The direction perpendicular to the vector $\Delta\mathbf{q}$ is slightly tilted $[\approx-1.6°\ (+1.6°)]$ with respect to the x axis [Fig. 5 (inset)]; this direction is roughly consistent with that of the observed dislocation glide. Although further study is necessary, this result suggests that there is a common physical-mathematical background for the stripe patterns in the wrinkle and convective systems. Meanwhile, the result also supports that the present defect motion is not specific to the configuration and details of the materials, e.g., Pt and the elastomer, which form a wrinkled surface.

Figure 4 also shows that the jump size depends on the degree of compression. Lower compression shows a larger deviation in θ until the jump to the optimal value, 0°. This result is consistent with the difference in the distribution of θ in Fig. 2(c). Namely, the result is understood from the fact

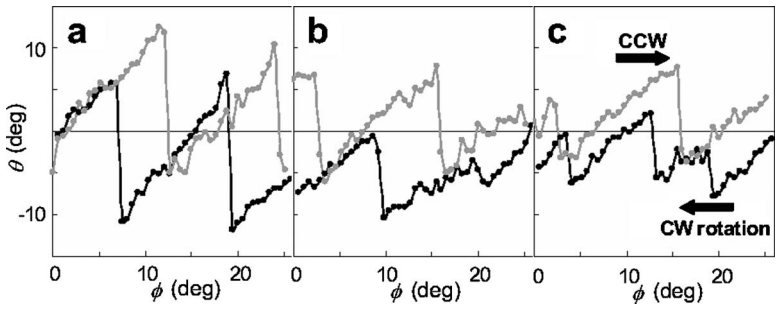

FIG. 4. Evolutions of θ at a fixed location on the steady states at compressive strains of (a) 5, (b) 7, and (c) 9% on the CW (solid lines) and CCW (gray lines) rotations.

that a lower compressive strain increases the possible number of system configurations.

The blurred stripe pattern in the images of θ [Figs. 3(d)–3(f)], which is a secondary structure, is closely related to the traces of the glide motion. The glides occur in the almost-fixed direction with respect to the x axis, and at the same time the sample is rotated. Therefore, the trace of the single glide ideally becomes a circular arc when the glide distance, d_g, for the unit change in ϕ is constant. However, it is difficult to observe the arcs because of the frequent annihilations of dislocation, the contrast change in the images of θ due to the sample rotation, and the large fluctuation in d_g. Nevertheless, the secondary structure indicates an important point that the simultaneous glides of dislocations tend to occur apart from each other in the direction perpendicular to the glide direction. That is, a dislocation disturbs the glides of other neighboring dislocations. As the dislocation glides, the neighboring stripe orientations as well as those on the gliding line are also changed. The reason for this is that the topological change usually modulates the neighbors somewhat within a characteristic distance to accommodate it. At such neighboring locations, the strain energy stored as a result of the change in the compression direction is relaxed somewhat. Thus, the energy to trigger the glide (as well as the formation of dislocations) at the neighbor of a dislocation becomes insufficient. This is probably the mechanism for the formation of the transient secondary structure.

During steady states, the glide events occur one after another at the locations with θ deviated from the compression direction. Such locations often lie between the newly formed secondary stripes with θ close to 0°. The formation of the pair of dislocations also occurs at such locations.

The distance between the transient secondary stripes in the θ image depends on the compressive strain. Lower compressive strain leads to a shorter distance. This indicates that the correlation distance between dislocations becomes shorter as the compressive strain decreases. This is visually interpreted by comparing the shapes of the dislocations at different compressive strains [Figs. 3(j)–3(l)]. The dislocations at high compression are elongated in the direction perpendicular to that of the compression. A similar difference in the shapes of dislocations can be found in the simulation of the convective rolls [28]. It is clear that the glide of the elongated dislocation at high compression changes θ over a large neighboring area. Thus, the distance depends on the compressive strain.

In summary, the stripe rearrangement under gradual changes in the compression direction is strongly related to the dislocation motions. The dislocations glide in specific lateral directions one after another over the sample surface to change the local stripe orientations back to the compression direction. The transient secondary structure observed as a blurred stripe pattern in the orientation image indicates the correlation between dislocations through the strain field.

We thank C. Kamaga, N. Uchida, and M. Aono for the informative discussions, E. Ito and T. Shiga for their help with the experiments. This work was partly supported by the grant-in-aid for young scientists (B) (No. 18750195) of the Ministry of Education, Culture, Sports, Science and Technology, Japan.

[1] M. Seul and D. Andelman, Science **267**, 476 (1995).
[2] C. Bowman and A. C. Newell, Rev. Mod. Phys. **70**, 289 (1998).
[3] P. Ball, *The Self-Made Tapestry* (Oxford University Press, New York, 2001).
[4] H. G. Allen, *Analysis and Design of Structural Sandwich Panels* (Pergamon, New York, 1969).
[5] D. Moldovan and L. Golubovic, Phys. Rev. Lett. **82**, 2884 (1999).
[6] E. Cerda and L. Mahadevan, Phys. Rev. Lett. **90**, 074302 (2003).
[7] R. Huang and Z. Suo, J. Appl. Phys. **91**, 1135 (2002).
[8] Z. Huang *et al.*, Phys. Rev. E **70**, 030601(R) (2004); , J. Mech. Phys. Solids **53**, 2101 (2005).
[9] N. Uchida, Physica D **205**, 267 (2005).
[10] N. Bowden *et al.*, Nature (London) **393**, 146 (1998); N. Bowden *et al.*, Appl. Phys. Lett. **75**, 2557 (1999); W. T. S. Huck *et al.*, Langmuir **16**, 3497 (2000).
[11] D. B. H. Chua *et al.*, Appl. Phys. Lett. **76**, 721 (2000).
[12] P. J. Yoo *et al.*, Adv. Mater. (Weinheim, Ger.) **14**, 1383 (2002); P. J. Yoo and H. H. Lee, Phys. Rev. Lett. **91**, 154502 (2003); P. J. Yoo *et al.*, *ibid.* **93**, 034301 (2004).
[13] N. Sridhar *et al.*, Appl. Phys. Lett. **78**, 2482 (2001).
[14] M. Watanabe *et al.*, J. Appl. Phys. **92**, 4631 (2002).
[15] T. Okayasu *et al.*, Adv. Funct. Mater. **14**, 1081 (2004).
[16] C. M. Stafford *et al.*, Nat. Mater. **3**, 545 (2004); C. Harrison *et al.*, Appl. Phys. Lett. **85**, 4016 (2004).
[17] J. Genzer and J. Groenewold, Soft Matter **2**, 310 (2006);
[18] J. Genzer *et al.*, Science **311**, 208 (2006);
[19] K. Efimenko *et al.*, Nat. Mater. **4**, 293 (2005).
[20] T. Ohzono and M. Shimomura, Phys. Rev. B **69**, 132202 (2004); Jpn. J. Appl. Phys., Part 1 **44**, 1055 (2005).
[21] T. Ohzono and M. Shimomura, Langmuir **21**, 7230 (2005).
[22] T. Ohzono *et al.*, Soft Matter **1**, 227 (2005); T. Ohzono and M. Shimomura, Colloids Surf., A (to be published).
[23] T. Ohzono and M. Shimomura, Phys. Rev. E **72**, 025203(R) (2005).
[24] The scenario is analogous to the bubble dynamics under shear. See M. Dennin and C. M. Knobler, Phys. Rev. Lett. **78**, 2485 (1997).
[25] D. A. Egolf *et al.*, Phys. Rev. Lett. **80**, 3228 (1998).
[26] The average amplitudes of wrinkles at these three strains are measured using atomic force microscopy, resulting in ~22, 47, and 65 nm. The quasilinear dependence of the amplitude on the compressive strain is consistent with the study by Harrison *et al.* [16].
[27] $|\mathrm{grad}(\theta)|=|(\partial\theta/\partial x, \partial\theta/\partial y)|$, where the differentials are substituted by the differences, $\Delta\theta$, in the x or y directions for actual calculations. When $\Delta\theta>90°$ (or $\Delta\theta<-90°$), $\Delta\theta$ is substituted by $180°-\Delta\theta$ (or $180°+\Delta\theta$) due to the C_2 symmetricity.
[28] E. Bodenschatz *et al.*, Physica D **32**, 135 (1988).
[29] S. Nasuno *et al.*, Phys. Rev. A **40**, 3457 (1989).